JOURNAL OF GEOPHYSICAL RESEARCH, VOL. 114, D06104, doi:10.1029/2008JD011244, 2009

Concentric gravity waves in the mesosphere generated by deep convective plumes in the lower atmosphere near Fort Collins, Colorado

Jia Yue,[1] Sharon L. Vadas,[2] Chiao-Yao She,[3] Takuji Nakamura,[4] Steven C. Reising,[1] Han-Li Liu,[5] Pete Stamus,[2] David A. Krueger,[3] Walter Lyons,[6] and Tao Li[7]

Received 3 October 2008; revised 5 December 2008; accepted 19 December 2008; published 18 March 2009.

[1] Gravity waves in the mesopause region (80–105 km) may induce perturbations in OH Meinal Band emissions at ~87 km. These perturbations can be observed by ground-based OH airglow imagers. In this paper, we present observations of concentric gravity waves (CGW) by the all-sky OH imager at Yucca Ridge Field Station (40.7°N, 104.9°W) near Fort Collins, Colorado. We find that expanding rings of concentric gravity waves were observed on 9 out of 723 clear nights from 2003 to 2008. In particular, on 11 May 2004, concentric rings were observed for ~1.5 h, with nearly perfect circular rings entirely in the field of view during the first 30 min. The centers of the concentric rings occurred at the geographic locations of two strong convective plumes which were active in the troposphere ~1 h earlier. We measured the horizontal wavelengths and periods of these gravity waves as functions of both radius and time. These results agreed reasonably well with the internal Boussinesq gravity wave dispersion relation with an assumed zero background wind. Similarly, for the other 8 cases, strong convective plumes occurred prior to the CGW observations near the apparent center of each of the arcs or rings. For the 7 out of the 9 cases, radiosonde data were available up to $z = 30–35$ km. These data showed that the wind speeds from the tropopause to ~30–35 km were smaller than ~20–30 m/s. Because 8 of the 9 cases occurred when the total horizontal mean winds were weak and because the horizontal winds below ~87 km were less than ~20 m/s on 11 May 2004 (according to radiosonde and TIME-GCM model data), we postulate that weak background horizontal winds are likely a necessary condition for gravity waves excited from convective overshooting to be observed as concentric arcs or rings in the OH layer.

Citation: Yue, J., S. L. Vadas, C.-Y. She, T. Nakamura, S. C. Reising, H.-L. Liu, P. Stamus, D. A. Krueger, W. Lyons, and T. Li (2009), Concentric gravity waves in the mesosphere generated by deep convective plumes in the lower atmosphere near Fort Collins, Colorado, *J. Geophys. Res.*, *114*, D06104, doi:10.1029/2008JD011244.

1. Introduction

[2] It is widely accepted that gravity waves play an important role in middle atmospheric dynamics. Along with topography and wind shear, convection is one of the dominant lower atmospheric mechanisms for the generation of gravity waves. Convection can generate gravity waves if upward moving air in the unstable troposphere "overshoots" the tropopause by ~1–3 km into the stably stratified stratosphere and then collapses back down to the tropopause [*Pierce and Coroniti*, 1966]. This rapid motion causes the excitation of a spectrum of gravity waves with widely varying spatial scales and frequencies [*Alexander et al.*, 1995; *Lane et al.*, 2001, 2003]. Some of these excited gravity waves have small scales and large amplitudes and may become nonlinear or reach critical levels below the stratopause [e.g., *Fritts and Alexander*, 2003; *Lane et al.*, 2003; *Lane and Sharman*, 2006]. Others are medium or large scale with larger phase speeds and smaller initial amplitudes, thereby enabling their propagation up to the mesopause and beyond. Several models developed in the last decade have simulated convectively generated gravity waves in three dimensions, greatly improving our understanding of the characteristics of gravity waves excited by this mechanism [*Piani et al.*, 2000; *Horinouchi et al.*, 2002; *Lane et al.*, 2003; *Alexander et al.*, 2004; *Vadas and Fritts*, 2009]. In general, all of these models show that convectively generated gravity waves have conically shaped phase surfaces when the intervening winds are small or zero. Therefore, although

[1]Department of Electrical and Computer Engineering, Colorado State University, Fort Collins, Colorado, USA.
[2]CoRA Division, NorthWest Research Associates, Boulder, Colorado, USA.
[3]Department of Physics, Colorado State University, Fort Collins, Colorado, USA.
[4]Research Institute for Sustainable Humanosphere, Kyoto University, Uji, Japan.
[5]National Center for Atmospheric Research, Boulder, Colorado, USA.
[6]FMA Research, Fort Collins, Colorado, USA.
[7]School of Earth and Space Sciences, University of Science and Technology of China, Anhui, China.

0148-0227/09/2008JD011244$09.00

the gravity waves are actually propagating upward and horizontally at the same time, in a horizontal plane at any given altitude, the waves and associated perturbations of trace species, such as the OH emission intensity, appear as outward, horizontally propagating concentric circular rings if the intervening winds are zero [*Vadas and Fritts*, 2009].

[3] In contrast to the common occurrence of convection in the troposphere, very few observations of concentric gravity waves (CGWs) have been reported from observations using ground-based airglow imagers [*Taylor and Hapgood*, 1988; *Sentman et al.*, 2003; *Suzuki et al.*, 2007] and spaceborne imagers [*Dewan et al.*, 1998]. However, nonconcentric gravity waves are believed to commonly propagate up into the mesopause region [e.g., *Fritts and Alexander*, 2003], where they are observed as nearly linear waves by sensitive OH imagers [e.g., *Swenson and Mende*, 1994; *Taylor et al.*, 1995; *Smith et al.*, 2000; *Ejiri et al.*, 2003; *Medeiros et al.*, 2003; *Nielsen et al.*, 2006]. Because intervening background winds can be strong and variable, linear gravity waves observed in the OH airglow layer can sometimes be correlated with their sources using reverse ray trace techniques [e.g., *Hung et al.*, 1978; *Waldock and Jones*, 1987; *Hecht et al.*, 2004; *Vadas et al.*, 2009a].

[4] This paper reports on 9 nights of midlatitude observations of CGWs by the Kyoto University OH all-sky imager, located at Yucca Ridge Field Station (YRFS), Colorado (40.7°N, 104.9°W), 20 km northeast of Fort Collins, Colorado. These CGWs were observed on the nights of 11 May 2004, 28 August 2005, 7 September 2005, 8 September 2005, 4 May 2007, 3 June 2008, 26 August 2008, 30 August 2008, and 4 September 2008. Here, we examine the convection which occurred prior to these events, as well as the tropospheric and lower stratospheric winds that are available from radiosondes. We choose one case in particular, 11 May 2004, for a more detailed study because of its high-quality data, long pattern duration, nearly circular rings, and clear ring patterns which contain little interference. The three main objectives of this paper are (1) to identify the convective plumes that excited the CGWs observed on 11 May 2004 and to show that convective plumes likely excited the CGWs observed in the other 8 cases; (2) to determine the periods and horizontal wavelengths of the CGWs temporally and spatially on 11 May 2004 and to compare them with the periods and scales predicted by the gravity wave Boussinesq dispersion relation under zero winds; and (3) to correlate the dates these CGWs were observed with the season and tropospheric/stratospheric winds. We suggest that a weak background wind in the stratosphere and lower mesosphere is a necessary condition for gravity waves to appear as concentric rings in the mesopause region in general and in the OH layer in particular. Note that a companion paper compares these observations on 11 May 2004 with theory using ray trace techniques through varying winds [*Vadas et al.*, 2009b]. These simulations include a mean background wind inferred from the HAMMONIA-GCM and lidar data at Fort Collins, Colorado, and therefore may be representative of the wind conditions on 11 May 2004.

2. Observations

[5] The OH all-sky imager was deployed by Kyoto University at YRFS, Colorado, in September 2003 [*Nakamura et al.*, 2005]. The imager is sensitive to the OH Meinel emissions between 795 nm and 1 μm, from the OH layer centered near 87 km altitude. The imager records one image every 2 min, limiting the temporal resolution of the analysis to 2 min. Because the buoyancy period is ~5 min, this observation rate is adequate.

[6] We examined all of the OH images recorded from fall 2003 to fall 2008 and found 723 clear nights of data during this 5 year period. CGWs were observed on 9 of these nights out of a total of 723 nights. We discuss the CGWs observed on 11 May 2004 first.

[7] Beginning at 0340 UT (2140 LT) on 11 May 2004 (UT day 132), curved wave patterns appeared to be moving away from a center in the southeast corner of the raw OH images. As time passed, the widths of the curved wave bands decreased with time. The waves disappeared completely at ~0510 UT (2310 LT). To investigate the concentric patterns in greater detail, two consecutive raw images were differenced to remove stars and the stationary background. Then, the difference images were unwrapped, i.e., geometrically corrected for lens distortion and mapped onto geographical coordinates following the algorithm described by *Garcia et al.* [1997], assuming the OH layer is at ~87 km altitude [*She and Lowe*, 1998]. This process transforms the curved patterns to nearly circular patterns on a flat field. Selected flat field OH images of the 11 May 2004 case are shown in Figure 1. In the 0350 UT image, for example, ~5 nearly perfect circles of bright wavefronts were observed. However, the inner 4 rings appear to have a different center than the outer ring at this time. We fit each ring with perfectly round circles of varying radii and centers, and overlay them as four red dashed circles (inner rings) and one blue dashed circle (the outer ring) in this image of Figure 1. The centers of the CGWs are denoted as red and blue solid dots, respectively. Note that the inner 4 circles have one center, and the outer ring has a different center; this implies that one convective plume is the source of the inner rings, while a second convective plume is the source of the outer ring. We also performed this procedure for the images at 0400 and 0430 UT in Figure 1, overlaying red and blue dashed circles on the inner and outer rings of each image, respectively. We see that the locations of the centers of the inner and outer rings, denoted by red and blue dots, respectively, are in approximately the same locations in each of the images; therefore, the geographic locations of the centers of the inner and outer CGWs are approximately fixed in time. We name the inner (red) and outer (blue) CGWs as CGW1 and CGW2, respectively. In section 3 we show that the centers of CGW1 and CGW2 correspond nearly exactly to the location of two deep convective plumes which were active ~1 h earlier, in good agreement with theory when the intervening winds are small [*Vadas et al.*, 2009b].

[8] Figure 2 shows OH images of the CGWs which were observed on the other 8 nights: on 28 August 2005, 7 September 2005, 8 September 2005, 4 May 2007, 3 June 2008, 26 August 2008, 30 August 2008, and 4 September 2008. These images display a rich variety of shapes and types of CGWs. In some cases, these CGWs appear as arcs rather than as rings. For example, the CGWs observed on 4 May 2007 and 3 June 2008 appear as arcs rather than as circles. Note that the arcs are quite distorted on many of

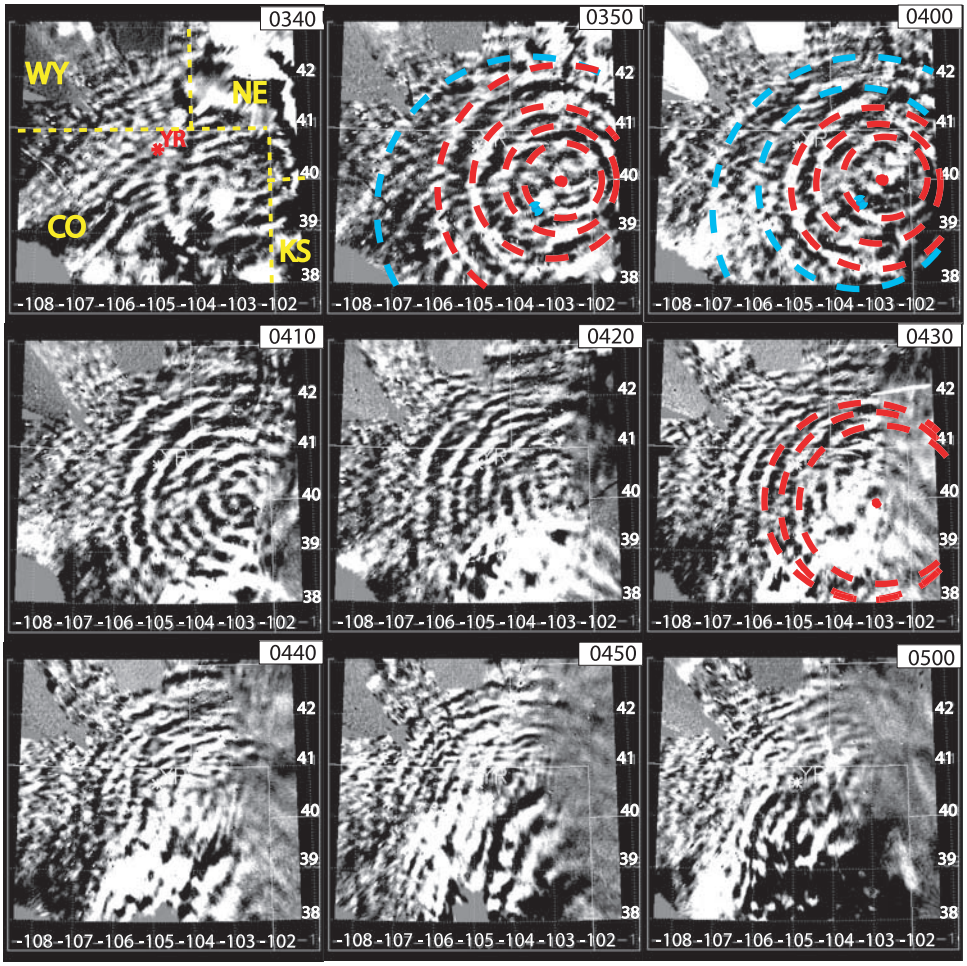

Figure 1. Time sequence of difference OH images in geographic coordinates from 0340 to 0500 UT on 11 May 2004. Figure 1 (top left) shows the state borders in yellow dashed lines between Wyoming, Nebraska, Colorado, and Kansas. The red star denotes the location of the OH imager at Yucca Ridge Field Station. The universal time of each image is shown the top right corner. Longitudes and latitudes are shown on the right and lower axes, respectively. The red and blue dashed circles denote CGW1 and CGW2, respectively, with estimated centers shown as red and blue solid dots.

these nights, implying large intervening winds [*Vadas et al.*, 2009b].

3. Convective Sources

[9] Gravity waves can be generated when a convective updraft "overshoots" the tropopause by 1–3 km into the stably stratified stratosphere [*Pierce and Coroniti*, 1966; *Larsen and Swartz*, 1982; *Lane et al.*, 2003]. On the night of 11 May 2004, the tropopause height was 12 km, as measured by the radiosonde launched from Denver/Stapleton, Colorado (39.75°N, 104.87°W). Figures 3a and 3b show the 0305 UT reflectivity images from the Goodland, Kansas (39.2°N, 101.4°W), National Weather Service WSR-88D NEXRAD Doppler radar. The convective overshoots are indicated by high reflectivities at altitudes 1–3 km above the tropopause. The centers of plume 1 at (40.0°N, 103.0°W) and plume 2 at (39.6°N, 103.8°W) are marked by red and white circles in Figure 3. Figure 3c shows the echo top chart with the same red and white circles at the same time. Here, the echo top is the largest altitude at which the reflectivity exceeds the minimum significant reflectivity of 18.5 dBZ, thereby showing the regions of convective overshoot. Figure 3c shows that the regions of convective overshoot occur at the same latitudes and longitudes (lat/long) as in the reflectivity images shown in Figures 3a and 3b. Using this information, as well as the results from the propagation time study we perform in section 4, we conclude that plume 1 and plume 2 are the sources of the CGW1 and CGW2 patterns, respectively. Model studies confirm that if the winds are zero, the apparent center of the concentric rings near the mesopause exactly coincide with the location of the convective plume [*Vadas and Fritts*, 2009]. If the intervening winds are much larger than ~20–30 m/s, however, the apparent center of the concentric rings are shifted significantly with respect to the location of the convective plume [*Vadas et al.*, 2009b]. We also note that similar "overshooting" updrafts are observed in visible-band GOES 12 satellite images, 3 or 4 h earlier (prior to sunset) for the same storm system but at different locations [*Vadas et al.*, 2009b].

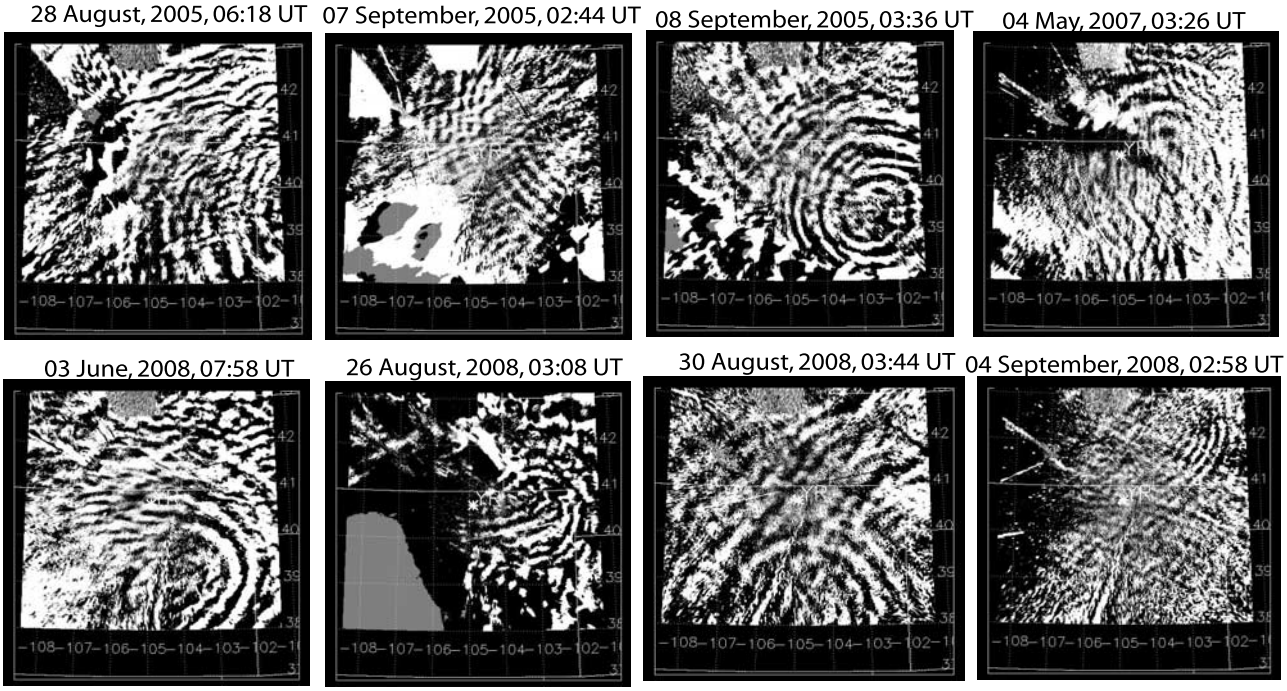

Figure 2. CGW OH images from eight nights. (top) The nights (from left to right) of 28 August 2005, 7 September 2005, 8 September 2005, and 4 May 2007, respectively. (bottom) The nights (from left to right) of 3 June 2008, 26 August 2008, 30 August 2008, and 4 September 2008, respectively.

[10] Figure 4 shows NEXRAD reflectivity measurements recorded prior to the observations of CGWs on the same nights shown in Figure 2. We also project some of the CGW arcs and rings from Figure 2 onto the corresponding radar maps. Despite the variation in propagation times between the radar maps in Figure 4 and the OH images in Figure 2, the approximate centers of the CGWs coincide with the location of the convective plumes reasonably well. Because these storms tend to move less than a few degrees in latitude or longitude per hour, and because these storms tend to create new convective updrafts continually by moving away from expended regions and into regions of higher convective available potential energy (CAPE), the CGWs shown in Figure 2 were likely excited by convective plumes from the same storm systems shown in Figure 4, although the actual convective plumes that excited the particular waves observed in Figure 2 may have occurred earlier or later than those shown in Figure 4, as we did not perform a detailed

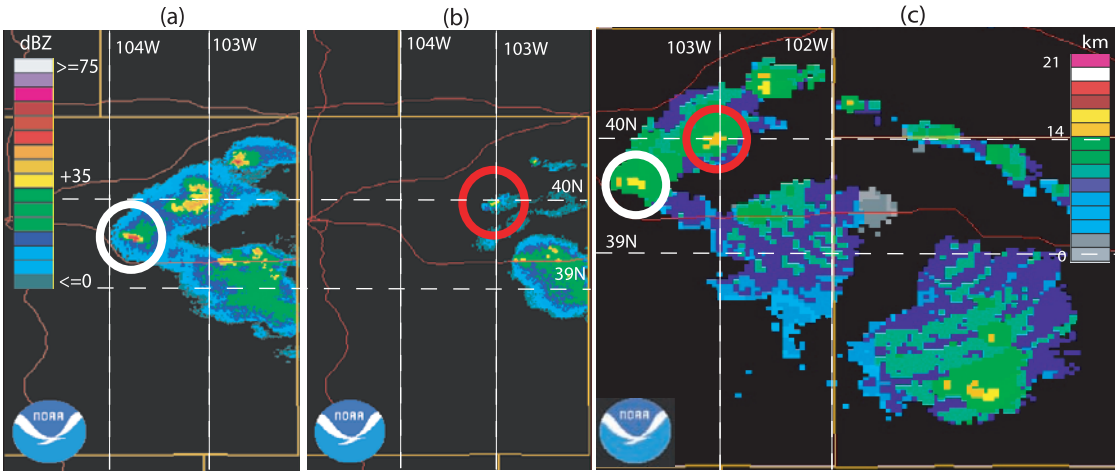

Figure 3. (a) and (b) NEXRAD reflectivity charts observed at Goodland, Kansas, at 0305 UT, on 11 May 2004, at elevation angles of 4.13° and 5.14°, respectively. (c) NEXRAD echo top height chart, also from Goodland, Kansas, at 0305 UT. Centers of the red and white circles are the locations of plumes 1 and 2, respectively. The altitudes of plumes 1 and 2 are 12 and 14 km, as determined from the distances and elevation angles in Figures 3b and 3a, respectively. The colors in the reflectivity charts (Figures 3a and 3b) indicate reflectivity in dB*Z*, and those in the echo top chart (Figure 3c) indicate altitude in km.

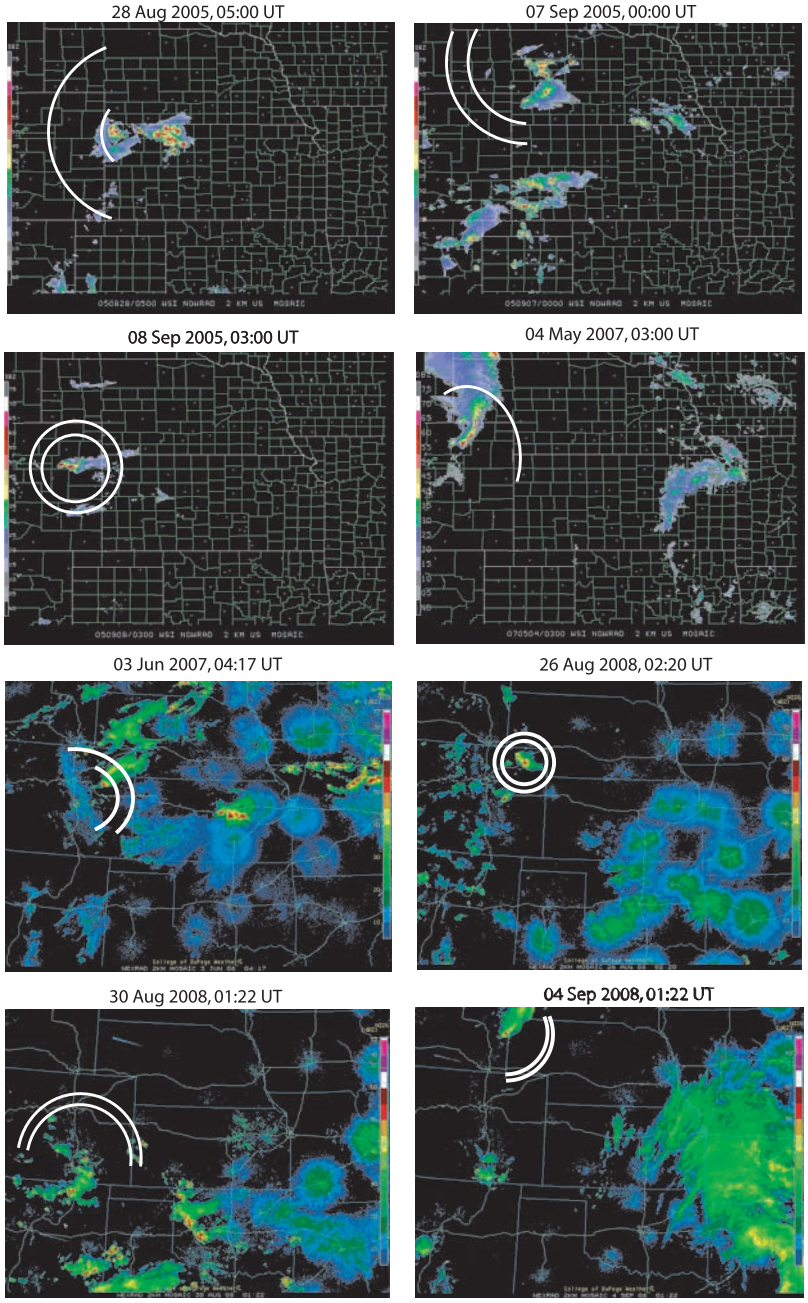

Figure 4. NEXRAD reflectivity maps recorded on the same nights on which CGWs were observed, as shown in Figure 2. Some of the arcs and rings of the CGWs in Figure 2 are projected onto the radar map as white arcs and circles.

comparison with wave propagation times and wavelengths, as we have done for the 11 May 2004 case (see section 4).

4. Analysis of CGWs Using the Gravity Wave Dispersion Relation

[11] Convective plumes excite CGWs with a large range of spatial and temporal scales [*Alexander et al.*, 1995; *Lane et al.*, 2003; *Vadas and Fritts*, 2009]. In this section, the spatial and temporal scales of the CGWs observed on 11 May 2004 are analyzed and compared with the predictions of the Boussinesq internal gravity wave dispersion relation using zero winds. The spatial and temporal scales (as a function of radius from the center of the CGW1), λ_h and τ, respectively, can be explained reasonably well with this dispersion relation. The Boussinesq gravity wave dispersion relation is [*Hines*, 1960]

$$\omega^2 = \frac{N^2 k_h^2}{k_h^2 + m^2} = N^2 \cos^2 \alpha, \tag{1}$$

where $\omega = 2\pi/\tau$ (assuming zero background wind), N, $k_h = 2\pi/\lambda_h$, and $m = 2\pi/\lambda_z$ are the intrinsic wave frequency (same as the apparent frequency assuming zero wind), buoyancy

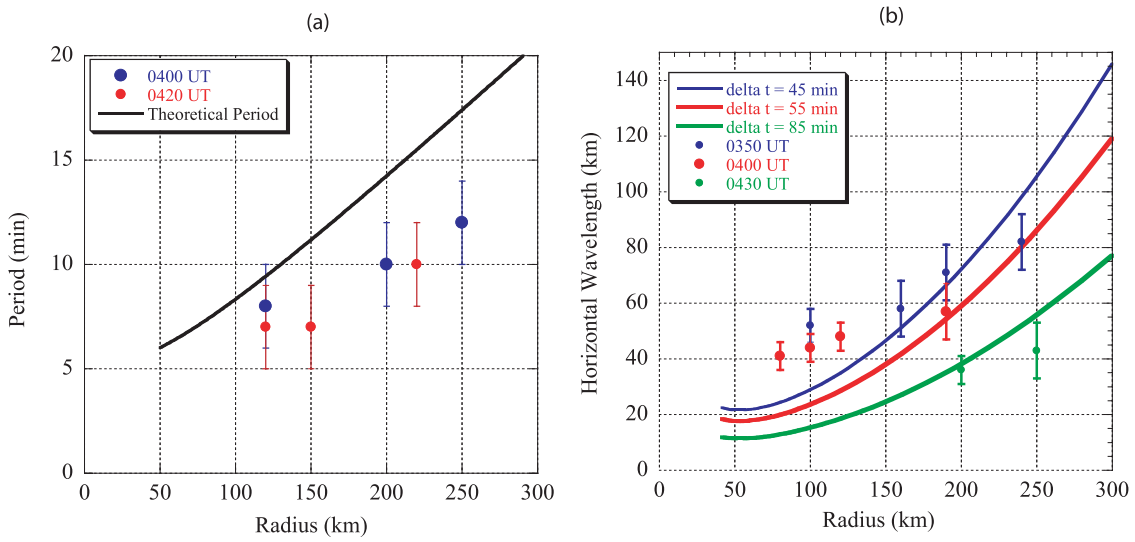

Figure 5. Temporal and spatial variations of CGW1 observed on 11 May 2004. (a) Observed wave periods (dots) compared to those calculated using dispersion relations (solid curve) as a function of radius: blue and red dots are the measured periods at 0400 and 0420 UT, respectively. (b) Horizontal wavelength λ_h as a function of both radius and time: dots are measured values. Blue, red, and green curves are calculated from the GW dispersion relation for propagation times Δt of 45, 55 and 85 min, respectively, between when the convective plume is generated near the tropopause and when CGWs were observed by the OH imager.

frequency, horizontal wave number, and vertical wave number of the wave, respectively. Additionally, α is the angle in a vertical plane between the vertical line and surfaces of constant phase of the CGW at a distance R away from the observed center of the CGW at ~87 km in altitude. Because the gravity wave generation mechanism considered here is convective overshoot, we assume that the gravity waves are launched from the tropopause. This is a good assumption because the fluid below the tropopause is generally unstable when convection is occurring, and therefore cannot support the propagation of gravity waves within the immediate plume vicinity. On the night of 11 May 2004, the tropopause is at 12 km altitude using the temperature profile measured by the Denver radiosonde. This altitude is typical at midlatitude during this season and is the same as that calculated by *Fovell et al.* [1992]. We denote Δz to be the vertical distance between the tropopause and the OH layer. Given that the average OH layer is at 87 km, Δz is $87 - 12 = 75$ km. Using the relation $\tan\alpha = R/\Delta z$, along with (1) with the assumption that N has a constant value of $2\pi/5$ min^{-1}, the period τ of a GW can be expressed in terms of R as

$$\tau = \frac{2\pi}{N}\sec\alpha = \frac{2\pi}{N}\sqrt{1+\frac{R^2}{\Delta z^2}}. \qquad (2)$$

Note that (2) implicitly assumes that the background winds are zero, the temperature is constant with altitude, and the Boussinesq assumption holds, i.e., that $\lambda_z \ll 4\pi H$, where $H \sim 7$ km is the density scale height. This simple relation (equation (2)) is plotted as a solid curve in Figure 5a. Note that this relation is independent of the propagation time because all gravity waves with the same frequency propagate at the same angle from the vertical line. The apparent period τ of CGW1 was measured using the sequential images in Figure 1. Since the imager records an image every 2 min, the uncertainty of the τ measurements is estimated to be ±2 min. Because CGW2 has a relatively large margin of error, it is excluded from Figure 5a. The periods of CGW1 are measured as a function of radius from the center of CGW1 along a line ~45° to the northwest of the center of CGW1, since the rings are the clearest along that line. The periods of CGW1 are measured at 0400 and 0420 UT, illustrated as blue and red dots, respectively, in Figure 5a, with error bars. Although both observed and predicted periods, τ, increase as the radius increases, equation (2) (with zero background winds and constant temperature with altitude) overpredicts the observed periods. Slightly better agreement with the observed periods is obtained via ray-tracing simulations where anelastic effects (i.e., not neglecting H) are included [*Vadas et al.*, 2009b]. The zero-wind assumption also affects the interpretation of the radius, R. When the winds are zero, the geographic location of the convective plume that excites the CGWs is the same as that of the center of the CGWs at the OH layer. However, when the intervening winds are much larger than ~20–30 m/s, the apparent center of the CGW is offset significantly from the location of the convective plume [*Vadas et al.*, 2009b]. In this case, plume 1 is at (40.0°N, 103.0°W), while the center of CGW1 is at (40.0°N, 102.8°W). Since the plume and the center of CGW1 are within 15 km of each other, the intervening winds are likely of order or smaller than ~20–30 m/s. Therefore, the measured radius of the observed rings is likely approximately the same as their horizontal distance from the convective plume that generated CGW1. In section 5, we show that the horizontal winds from the radiosonde and the thermosphere ionosphere mesosphere

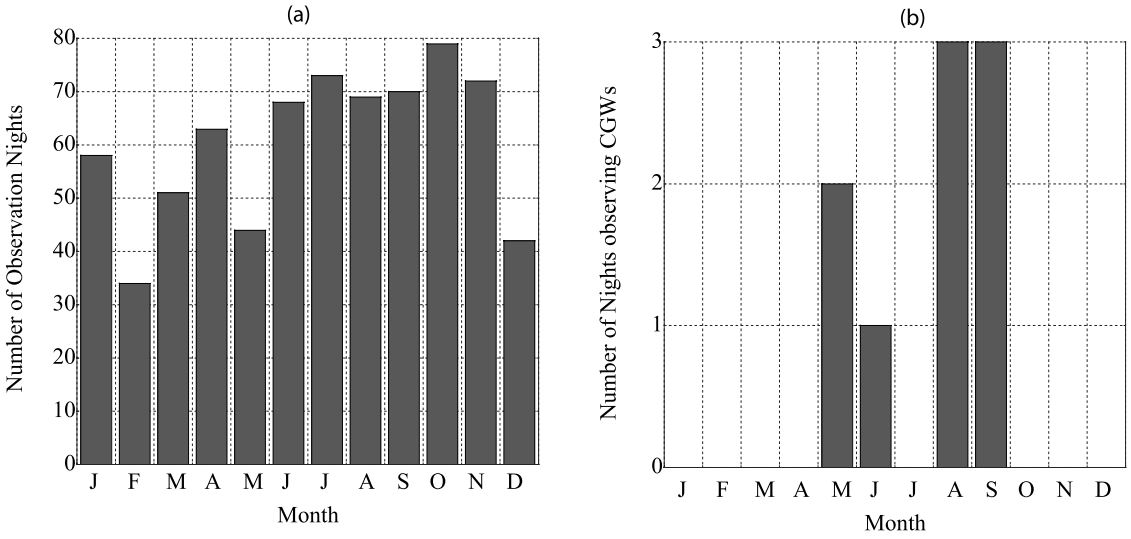

Figure 6. (a) Monthly distribution of clear observation nights of the OH imager from 2003 to 2008. (b) Monthly distribution of CGW observations during the same period.

electrodynamics-general circulation model (TIME-GCM) are smaller than 20 m/s on 11 May 2004. Therefore, the zero-wind assumption we use here is reasonable.

[12] The observed horizontal wavelengths at the OH layer altitude of ~87 km depend on the propagation time, Δt, of the gravity waves from their excitation by the convective plume to their observation location within the OH layer. This propagation time in turn depends on the vertical group velocity c_{gz}:

$$c_{gz} = \frac{\partial \omega}{\partial m} = -\frac{N k_h m}{\left(k_h^2 + m^2\right)^{3/2}} = -\frac{N}{k_h}\frac{\tan\alpha}{\sec^3\alpha}, \qquad (3)$$

in which the relations $m = k_h \tan\alpha$, and, $k_h^2 + m^2 = k_h^2 \sec^2\alpha$ have been used. Again assuming zero winds, the time it takes for a gravity wave to propagate from the tropopause to the OH layer is $\Delta t = \Delta z / |c_{gz}|$. Taking the absolute value of (3) and substituting $\Delta z / \Delta t$ for c_{gz}, the gravity wave horizontal wavelength, λ_h, as a function of radius, R, and propagation time, Δt, is:

$$\lambda_h = \frac{2\pi R^2 (1 + \Delta z^2 / R^2)^{3/2}}{N \Delta z \Delta t}. \qquad (4)$$

We measure the average horizontal wavelength, λ_h, of CGW1 as a function of radius at 0350, 0400 and 0430 UT along a line ~45° toward the northwest of the center of CGW1. (This is the same line as was used to measure the observed periods of CGW1). The λ_h, values are measured to be the distance between two consecutive wave crests or troughs in the images. The radius R used in each measurement is then the midpoint between two crests or two troughs. The uncertainties in λ_h, are estimated from the errors caused by wave interference and noise. These measurements are plotted as dots in Figure 5b. Since plume 1 overshot the tropopause at 0305 UT, the corresponding gravity wave propagation times, Δt, are 45, 55 and 85 min for the OH imager observation times of 0350, 0400 and 0430 UT, respectively. The horizontal wavelengths derived from (4) as a function of R for Δt = 45, 55 and 85 min are plotted as blue, red, and green solid lines, respectively, in Figure 5b. The observed horizontal wavelengths for CGW1 at different Δt are again in general agreement with the gravity wave dispersion relation for zero winds, since λ_h increases as R increases at a given Δt, and λ_h decreases with time at a fixed radius R [*Vadas and Fritts*, 2009]. A discrepancy exists because the observed λ_h is larger than the zero wind theory results for R < 150 km and is typically smaller for R > 200 km. We have also determined λ_h for CGW2 at 0400 for two radii from its center (blue dot in Figure 1): they are 77 and 102 km for R = 190 km and 260 km, respectively. Within error bars, these values are consistent with the simple prediction (red curve) in Figure 5b. Better agreement is obtained for radii R < 150 km using realistic convective spectra, realistic winds, and an anelastic dispersion relation [*Vadas et al.*, 2009b].

[13] The vertical wavelengths λ_z of CGW1 are calculated using (1) with the assumption that the background winds are zero. The resulting vertical wavelengths are ~20–40 km. This is greater than twice the vertical thickness (~8 km) of the OH emission layer. From *Liu and Swenson* [2003], the cancellation factor for OH emission and for vertical wavelengths of 20–40 km is 2–3. Therefore, we estimate that the OH airglow intensity perturbations are reduced by ~20–45% for CGW1 compared to GWs with infinitely large vertical wavelengths.

5. Seasonal and Background Wind Conditions and CGW Observations

[14] Although gravity waves are often observed by airglow imagers as quasi-monochromatic, quasi-linear, parallel-phase fronts with horizontal wavelengths limited by the typical range of resolution of all-sky imagers (20–500 km), concentric gravity waves are rarely observed. The monthly distribution of the 723 clear nights of data from September 2003 to September 2008 is shown as a histogram in Figure 6a. The observations are fairly uniform throughout the year. Figure 6b shows the monthly distribution of CGW

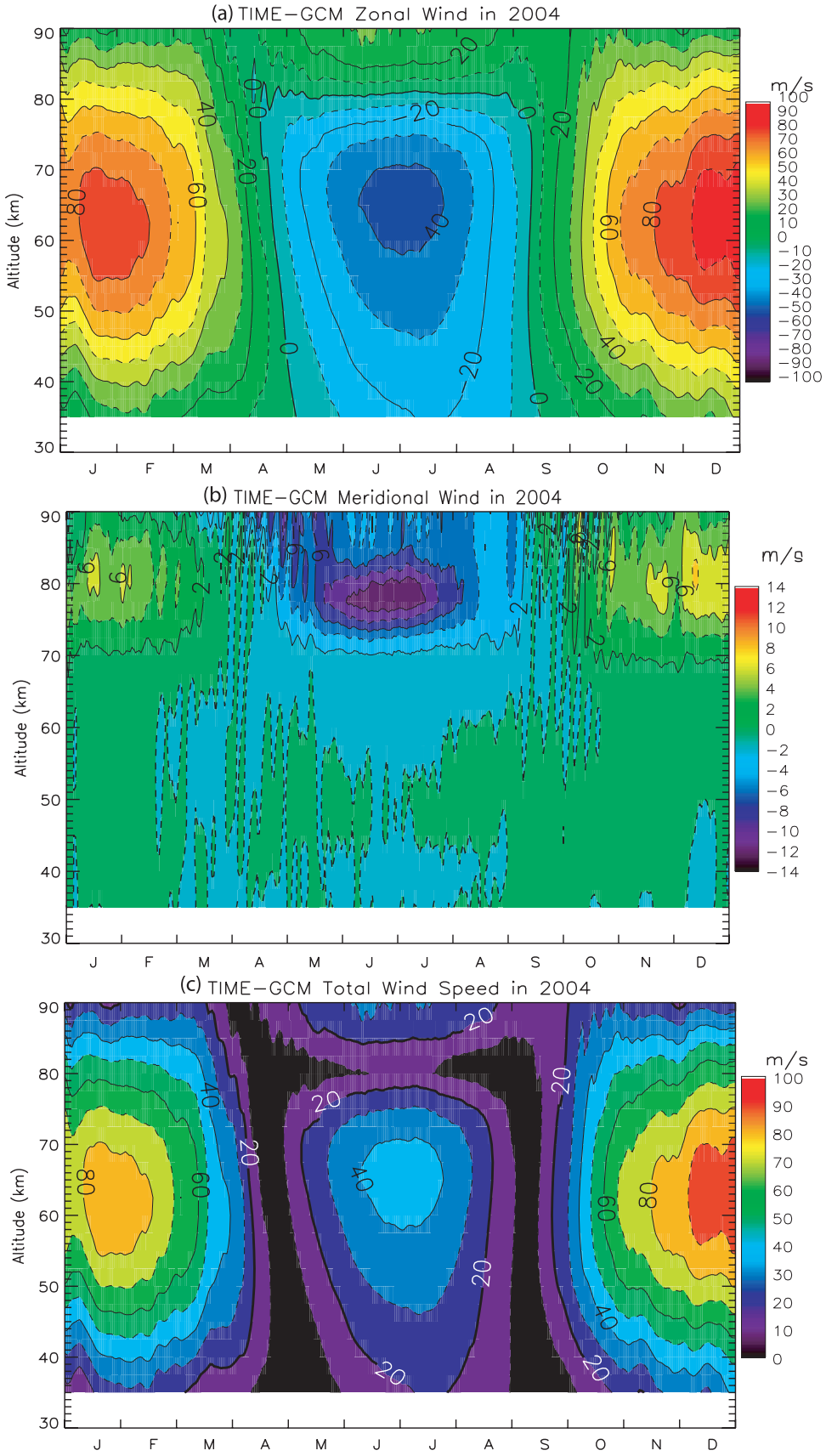

Figure 7. TIME-GCM zonal mean horizontal wind climatology at 42°N for 2004. (a) Zonal wind. (b) Meridional wind. (c) Total horizontal wind speed.

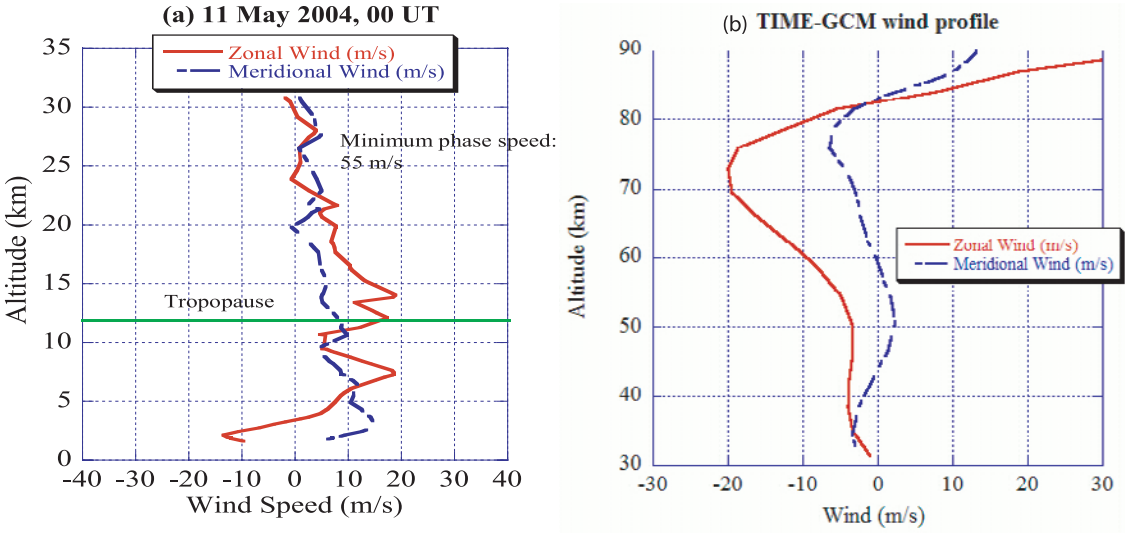

Figure 8. (a) Radiosonde wind (0–30 km) and (b) TIME-GCM wind (30–90 km) on the night of 11 May 2004. In Figure 7a, the height of the tropopause is marked by a green line in each case. The minimum horizontal phase speeds of the CGWs are labeled.

observations. Nearly concentric CGWs were observed by the Yucca Ridge OH imager only on 11 May 2004, 28 August 2005, 7 and 8 September 2005, 4 May 2007, 3 June 2008, 26 and 30 August 2008, and 4 September 2008. Therefore, 8 out of these 9 events were observed ~2 months after the spring equinox and ~0.5–1 months before the fall equinox. Comparing with Figure 6a, we see that the seasonal distribution of CGWs is not caused by a skewed monthly distribution of the clear-night imager data. The occurrence frequency of CGW observations is very low (9/723 ≈ 1.5%). The peaks of CGW observations occur in May and in August–September, which are ~3–4 months apart.

[15] We now discuss a possible reason as to why the CGWs are primarily observed in May and in August–September. The zonal and meridional mean winds between 35 and 90 km at 42°N are shown in Figures 7a and 7b from a recent climatology run of the TIME-GCM. The zonal mean winds are weaker than 20 m/s (because they switch direction) from 15 April to 15 May and 15 August to 15 September, which are ~4 months apart [*Roble*, 1995]. Therefore, if the planetary and tidal waves happen to be weak (which may only occur on certain days and at certain local times) and if the mean winds above the tropopause are weak, then the total winds from the tropopause to the upper mesosphere may be weak. (We show that this is the case for the 11 May 2004 example below using radiosonde and TIME-GCM data.) As suggested by *Suzuki et al.* [2007], weak horizontal winds appear to be a necessary condition for the observation of CGWs in the mesopause region. The total horizontal wind speed is shown in Figure 7c, obtained from Figures 7a and 7b. Weak total winds with speeds < 20 m/s are seen from 15 April to 15 May and from 15 August to 15 September. The weak climatological winds may explain why the occurrence distribution in Figure 6b is double peaked during these spring and fall months. Additionally, peak thunderstorm season over eastern Colorado is from late April through early September. Therefore, the seasonal dependence of convective sources near YRFS, Colorado, constrains the occurrence of CGWs to be from May to September.

[16] As shown in Figure 6b, 8 of the 9 CGW events were observed in May or late August/early September when the total climatological wind speed above the tropopause is low. The CGWs reported by *Sentman et al.* [2003] occurred on 19 August at a nearby location with a similar latitude/longitude.

[17] The only case of the 9 CGW observations that did not occur during the period when the mean climatological winds are <20 m/s was 3 June 2008. On that night, however, it is possible that the total wind (with the planetary wave, tidal, and other wave contributions) was unusually weak.

[18] Since tidal and planetary waves, as well as lower stratospheric winds from weather systems, can significantly increase the hourly winds from the weak monthly mean wind, we examine the wind profiles for these 9 cases. Figures 8a and 8b show the horizontal wind profiles at 0000 UT on 11 May 2004 from the ground to 90 km. Figure 8a shows the Denver radiosonde winds, while Figure 8b shows the TIME-GCM winds at the time of the CGW observations. The maximum wind speed below 87 km is no greater than ±20 m/s. Therefore, we infer that the combined planetary and tidal winds are small at the time the CGWs were observed on 11 May 2004.

[19] The winds observed by the same Denver radiosondes (with altitude ranges of ~0–30 km) are shown in Figure 9 for the other nights when 6 of the CGWs were observed. The sounding failed above the tropopause on 26 August 2008; no radiosonde data are available on 30 August 2008 and 4 September 2008. These soundings are only available at 0000 and 1200 UT. Only the soundings at 0000 UT are shown because the 0000 UT soundings are closer to the times of the convection. For all of these cases, the horizontal wind speeds above the tropopause (where the CGWs propagate) were smaller than ~30 m/s. The apparent minimum horizontal phase speeds of these CGWs labeled

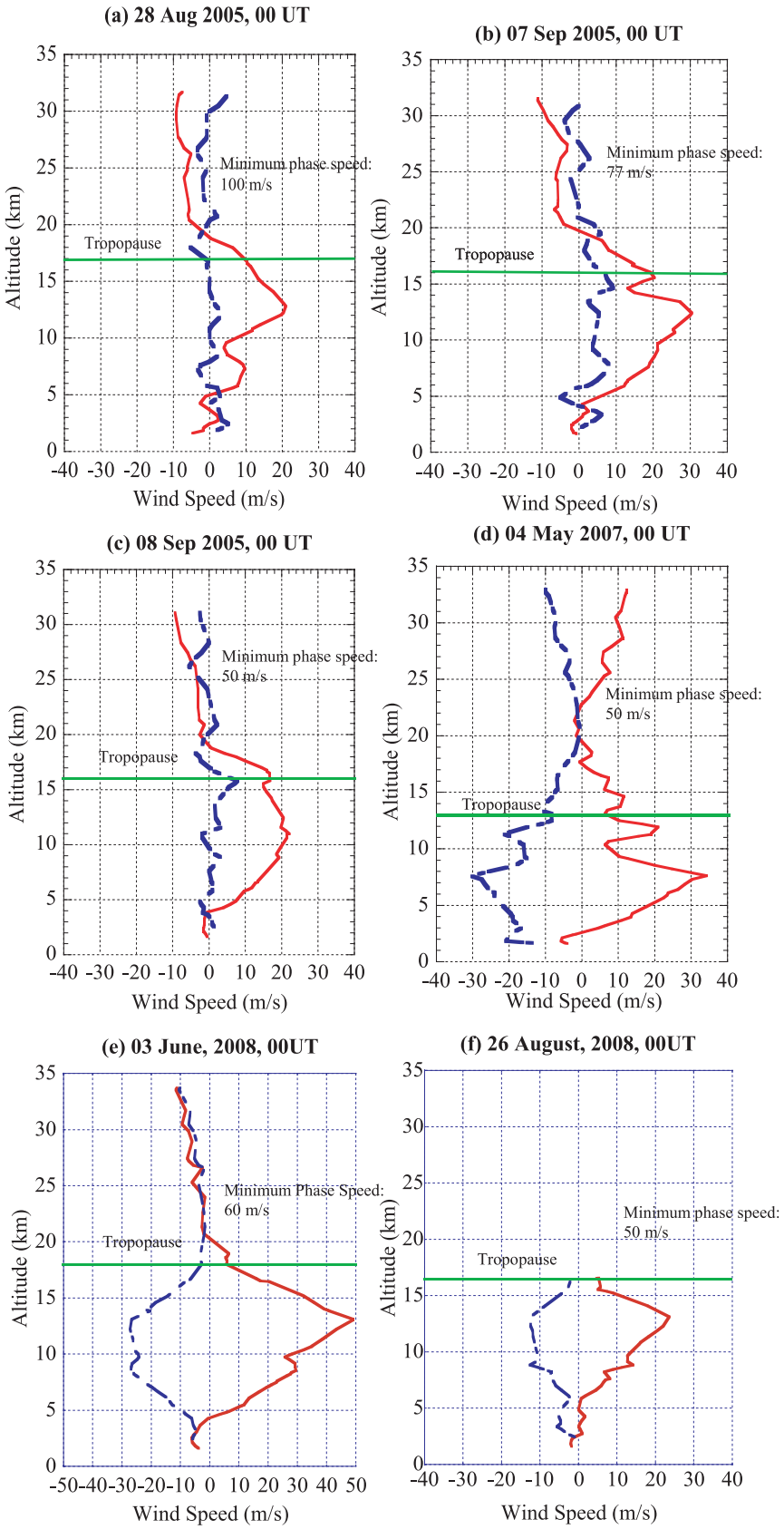

Figure 9. Radiosonde wind profiles as Figure 8a on the nights of CGW observations on (a) 28 August 2005, (b) 7 September 2005, (c) 8 September 2005, (d) 4 May 2007, (e) 3 June 2008, and (f) 26 August 2008. Profiles at Denver/Stapleton Station (39.75°N, 104.87°W), the closest to YRFS, are unavailable for 30 August and 4 September 2008.

on each graph are 50–120 m/s, much larger than the winds from 12 to 30 km. Although obtaining TIME-GCM winds for these 8 cases is beyond the scope of this paper, the radiosonde data along with the detailed 11 May 2004 data/model winds provide evidence that weak background horizontal winds permit the propagation of CGWs into the mesopause region with relatively little filtering and distortion at those altitudes, allowing the CGWs to appear as rings or arcs in the OH layer. Indeed, *Vadas et al.* [2009b] find that the concentric rings near the mesopause are "squashed" or arc-like if the intervening zonal winds are much larger than ~20–30 m/s and the meridional winds are zero. If the intervening winds are zero, the gravity waves appear as perfectly concentric rings near the mesopause. If the intervening winds are less than ~30 m/s, the gravity waves appear mostly as concentric rings, although portions of the rings may disappear at late times because of wave reflection and critical level absorption.

[20] We now connect the shape of the arcs and concentric CGWs in Figures 1 and 2 with the horizontal winds in the troposphere in Figure 8a and 9. On 11 May 2004, 8 September 2005, and 26 August 2008, the CGWs are 360° circular rings, while on 4 May 2007 and 3 June 2008, the CGWs are arcs. Simulations show that if a convective plume is moving vertically through zero wind, then perfectly circular rings of gravity waves are generated [*Vadas and Fritts*, 2009; *Vadas et al.*, 2009b]. However, convective plumes in a wind shear environment result in the generation of an asymmetric spectrum of gravity waves, with gravity waves propagating mainly in the rearward direction of the storm propagation direction [*Fovell et al.*, 1992; *Lane et al.*, 2001]. Additionally, concentric CGWs propagating through large-scale winds (such as the QBO) become anisotropic, resulting in only half of the rings being visible [*Piani et al.*, 2000]. Finally, a plume moving through a tropospheric wind shear tilts at an angle in the vertical [e.g., *Marwitz and Berry*, 1971]. Ray trace simulations show that tilted plumes with zero wind above the tropopause create an anisotropic spectrum of GW which appear as arcs, not concentric rings (S. L. Vadas, personal communication, 2008). As shown in Figures 9d and 9e, large eastward zonal and southward meridional wind shears exist in the upper troposphere on both 4 May 2007 and 3 June 2008. This may partially account for the CGW appearing as arcs in the OH airglow layer on these nights (see Figure 2). On days when circular wave patterns are observed (e.g., 11 May 2004, 8 September 2005, and 26 August 2008 from Figures 1 and 2), the wind shear in the upper troposphere is relatively small (see Figures 8a, 9c, and 9f).

6. Conclusion

[21] This paper reports on the observations of CGWs on 9 nights using an all-sky OH imager at the Yucca Ridge Field Station (YRFS) near Fort Collins, Colorado. These observations consisted of nearly perfect circles, "squashed" rings, and arcs. We found that in every case, deep convection was present an hour or more prior to the observed event near the apparent center of the CGW. We also found that the wind below 30–35 km was weak, less than 20 m/s, using radiosonde data.

[22] We also performed a detailed study on 11 May 2004. On that night, two nearly circular concentric gravity waves were observed, with different centers. Strong convective updrafts that "overshot" the tropopause were identified as the sources of the two CGWs. The locations of these convective plumes coincide with the centers of the CGWs to within 0.2° in lat/long. We also found that the horizontal winds between the tropopause and mesopause are small, using radiosonde and TIME-GCM model data. The modeling study in the companion paper confirms that the centers of the CGWs coincide with that of the convective plumes when the intervening winds are weak [*Vadas et al.*, 2009b]. That model study also finds that the CGWs appear as concentric rings for climatological April winds.

[23] We also find that the observed horizontal wavelengths on 11 May 2004 as a function of radius and time are in very good agreement with the predictions of the Boussinesq gravity wave dispersion relation (with assumed zero winds and constant temperatures) for radii between 150 and 200 km. The apparent periods are in reasonable agreement. Somewhat better agreement is obtained when anelastic effects and varying winds are employed instead [*Vadas et al.*, 2009b]. Additionally, realistic temperatures and detailed plume dynamics may further improve the agreement between observations and theory.

[24] By studying all 9 cases in which nearly concentric CGWs were observed by the OH imager at YRFS, we conclude that the occurrence frequency is small, about 9/723, or about 1.25%. Because of the strong seasonal occurrence after the spring equinox and just prior to the fall equinox, which coincides with times when the mean background wind is nearly zero, weak mean background wind between the tropopause and mesopause was hypothesized to be a necessary condition for enabling CGWs to propagate upward as concentric rings to the OH airglow layer. Additionally, the companion model study showed that the gravity waves appear as circular CGWs only when the total background winds between the tropopause and mesopause are weak [*Vadas et al.*, 2009b]. Thus, we hypothesize that during the times when the 9 CGW events occurred, the mean wind as well as the winds from tides and planetary waves were likely small. Indeed, we found this to be the case on 11 May 2004, using radiosonde and TIME-GCM data. A larger data set with better background wind information will allow this hypothesis to be tested further. Since CGWs are generated by strong updrafts in convective clouds, these same clouds may block the view of the OH imager and reduce the chance of observing CGWs in the OH layer. Also, CGWs with vertical wavelengths smaller than 10 km cannot be observed by OH airglow imagers due to the "cancellation factor" effect as the CGWs propagate through the OH layer [*Liu and Swenson*, 2003]. All of these factors may contribute to the overall low observation frequency reported here, in addition to the winds likely needing to be small. The images in Figures 1 and 2 coupled with the eastward tropospheric winds in Figures 8a and 9 suggest that an imager located upwind of a convectively active region is more favorable for CGW observation. In general, in northeastern Colorado, the tropospheric winds tend to be westerly (toward the east), and the winds may blow the convective clouds eastward out of the YRFS imager field of view, enabling a relatively higher rate of

observation of CGWs for northeastern Colorado than for other imager locations.

[25] **Acknowledgments.** The work at Colorado State University; Colorado Research Associates; Kyoto University; and FMA Research is supported by grants from NASA, NNX07AB64G, and NSF, ATM-0545221; from NSF, ATM-0537311; for Scientific Research (B) 14403008 and 20403011 from MEXT, Japan; and NSF, ATM-0649034, respectively. The authors thank the two anonymous reviewers for their helpful comments.

References

Alexander, M. J., J. R. Holton, and D. R. Durran (1995), The gravity wave response above deep convection in a squall line simulation, *J. Atmos. Sci.*, *52*(12), 2212–2226, doi:10.1175/1520-0469(1995)052<2212:TGWRAD>2.0.CO;2.

Alexander, M. J., P. T. May, and J. H. Beres (2004), Gravity waves generated by convection in Darwin area during the Darwin Area Wave Experiment, *J. Geophys. Res.*, *109*, D20S04, doi:10.1029/2004JD004729.

Dewan, E. M., R. H. Picard, R. R. O'Neil, H. A. Gardiner, J. Gibson, J. D. Mill, E. Richards, M. Kendra, and W. O. Gallery (1998), MSX satellite observations of thunderstorm-generated gravity waves in mid-wave infrared images of the upper stratosphere, *Geophys. Res. Lett.*, *25*, 939–942, doi:10.1029/98GL00640.

Ejiri, M. K., K. Shiokawa, T. Ogawa, K. Igrashi, T. Nakamura, and T. Tsuda (2003), Statistical study of short-period gravity waves in OH and OI nightglow images at two separated sites, *J. Geophys. Res.*, *108*(D21), 4679, doi:10.1029/2002JD002795.

Fovell, R., D. Durran, and J. R. Holton (1992), Numerical simulations of convectively generated stratospheric gravity waves, *J. Atmos. Sci.*, *49*, 1427–1442, doi:10.1175/1520-0469(1992)049<1427:NSOCGS>2.0.CO;2.

Fritts, D. C., and M. J. Alexander (2003), Gravity wave dynamics and effects in the middle atmosphere, *Rev. Geophys.*, *41*(1), 1003, doi:10.1029/2001RG000106.

Garcia, F. J., M. J. Taylor, and M. C. Kelley (1997), Two-dimensional spectral analysis of mesospheric airglow image data, *Appl. Opt.*, *36*(29), 7374–7385, doi:10.1364/AO.36.007374.

Hecht, J. H., S. Kovalam, P. T. May, G. Mills, R. A. Vincent, R. L. Walterscheid, and J. Woithe (2004), Airglow imager observations of atmospheric gravity waves at Alice Springs and Adelaide, Australia, during the Darwin Area Wave Experiment (DAWEX), *J. Geophys. Res.*, *109*, D20S05, doi:10.1029/2004JD004697.

Hines, C. O. (1960), Internal atmospheric gravity waves at ionospheric heights, *Can. J. Phys.*, *38*, 1441–1481.

Horinouchi, T., T. Nakamura, and J.-I. Kosaka (2002), Convectively generated mesoscale gravity waves simulated throughout the middle atmosphere, *Geophys. Res. Lett.*, *29*(21), 2007, doi:10.1029/2002GL016069.

Hung, R. J., T. Phan, and R. E. Smith (1978), Observations of gravity waves during the extreme tornado outbreak of 3 April 1974, *J. Atmos. Terr. Phys.*, *40*, 831–843, doi:10.1016/0021-9169(78)90033-8.

Lane, T. P., and R. D. Sharman (2006), Gravity wave breaking, secondary wave generation, and mixing above deep convection in a three-dimensional cloud model, *Geophys. Res. Lett.*, *33*, L23813, doi:10.1029/2006GL027988.

Lane, T. P., M. J. Reeder, and T. L. Clark (2001), Numerical modeling of gravity waves generated by deep tropical convection, *J. Atmos. Sci.*, *58*, 1249–1274, doi:10.1175/1520-0469(2001)058<1249:NMOGWG>2.0.CO;2.

Lane, T. P., R. D. Sharman, T. L. Clark, and H.-M. Hsu (2003), An investigation of turbulence generation mechanisms above deep convection, *J. Atmos. Sci.*, *60*, 1297–1321, doi:10.1175/1520-0469(2003)60<1297:AIOTGM>2.0.CO;2.

Larsen, M. F., and W. E. Swartz (1982), Gravity-wave generation by thunderstorms observed with a vertically pointing 430 MHz radar, *Geophys. Res. Lett.*, *9*(5), 571–574, doi:10.1029/GL009i005p00571.

Liu, A. Z., and G. R. Swenson (2003), A modeling study of O_2 and OH airglow perturbations induced by atmospheric gravity waves, *J. Geophys. Res.*, *108*(D4), 4151, doi:10.1029/2002JD002474.

Marwitz, J. D., and E. X. Berry (1971), The airflow within the weak echo region of an Alberta hailstorm, *J. Appl. Meteorol.*, *10*, 487–492, doi:10.1175/1520-0450(1971)010<0487:TAWTWE>2.0.CO;2.

Medeiros, A. F., M. J. Taylor, H. Takahashi, P. P. Batista, and D. Gobbi (2003), An investigation of gravity wave activity in the low-latitude upper mesosphere: Propagation direction and wind filtering, *J. Geophys. Res.*, *108*(D14), 4411, doi:10.1029/2002JD002593.

Nakamura, T., T. Fukushima, T. Tsuda, C. Y. She, B. P. Williams, D. Krueger, and W. Lyons (2005), Simultaneous observation of dual-site airglow imagers and a sodium temperature-wind lidar, and effect of atmospheric stability on the airglow structure, *Adv. Space Res.*, *35*, 1957–1963, doi:10.1016/j.asr.2005.05.102.

Nielsen, K., M. J. Taylor, P. D. Pautet, D. C. Fritts, N. Mitchell, C. Beldon, W. Singer, F. J. Schmidlin, and R. A. Goldberg (2006), Propagation of short-period gravity waves at high-latitudes during the MaCWAVE winter campaign, *Ann. Geophys.*, *24*, 1–17.

Piani, C., D. Durran, M. J. Alexander, and J. R. Holton (2000), A numerical study of three-dimensional gravity waves triggered by deep tropical convection and their role in the dynamics of the QBO, *J. Atmos. Sci.*, *57*(22), 3689–3702, doi:10.1175/1520-0469(2000)057<3689:ANSOTD>2.0.CO;2.

Pierce, A. D., and S. C. Coroniti (1966), A mechanism for the generation of acoustic-gravity waves during thunderstorm formation, *Nature*, *210*, 1209–1210, doi:10.1038/2101209a0.

Roble, R. G. (1995), Energetics of the mesosphere and thermosphere, in *The Upper Mesosphere and Lower Thermosphere: A Review of Experiment and Theory*, *Geophys. Monogr. Ser.*, vol. 87, edited by R. M. Johnson and T. L. Killeen, pp. 1–20, AGU, Washington, D. C.

Sentman, D. D., E. M. Wescott, R. H. Picard, J. R. Winick, H. C. Stenbaek Nielsen, E. M. Dewan, D. R. Moudry, F. T. Sao Sabbas, M. J. Heavner, and J. Morrill (2003), Simultaneous observations of mesospheric gravity waves and sprites generated by a midwesterm thunderstorm, *J. Atmos. Terr. Phys.*, *65*, 537–550, doi:10.1016/S1364-6826(02)00328-0.

She, C.-Y., and R. P. Lowe (1998), Seasonal temperature variations in the mesopause region at mid-latitude: Comparison of lidar and hydroxyl rotational temperatures using WINDII/UARS OH height profiles, *J. Atmos. Terr. Phys.*, *60*(16), 1573–1583, doi:10.1016/S1364-6826(98)00082-0.

Smith, S. M., M. Mendillo, J. Baumgardner, and R. R. Clark (2000), Mesospheric gravity wave imaging at subauroral site: First results from Millstone Hill, *J. Geophys. Res.*, *105*(A12), 27,119–27,130, doi:10.1029/1999JA000343.

Suzuki, S., K. Shiokawa, Y. Otsuka, T. Ogawa, K. Nakamura, and T. Nakamura (2007), A concentric gravity wave structure in the mesospheric airglow images, *J. Geophys. Res.*, *112*, D02102, doi:10.1029/2005JD006558.

Swenson, G. R., and S. B. Mende (1994), OH emissions and gravity waves (including a breaking wave) in all-sky imagery from Bear Lake, Utah, *Geophys. Res. Lett.*, *21*(20), 2239–2242, doi:10.1029/94GL02112.

Taylor, M. J., and M. A. Hapgood (1988), Identification of a thunderstorm as a source of short period gravity waves in the upper atmospheric nightglow emissions, *Planet. Space Sci.*, *36*, 975–985, doi:10.1016/0032-0633(88)90035-9.

Taylor, M. J., M. B. Bishop, and V. Taylor (1995), All-sky measurements of short period waves imaged in the OI (557.7 nm), Na (589.2 nm) and near infrared OH and O2 (0,1) nightglow emissions during the ALOHA-93 campaign, *Geophys. Res. Lett.*, *22*(20), 2833–2836, doi:10.1029/95GL02946.

Vadas, S. L., and D. C. Fritts (2009), Reconstruction of the gravity wave field from convective plumes via ray tracing, *Ann. Geophys.*, *27*, 147–177.

Vadas, S. L., M. J. Taylor, P.-D. Pautet, P. Stamus, D. C. Fritts, H.-L. Liu, F. T. Sao Sabbas, V. T. Rampinelli, P. Batista, and H. Takahashi (2009a), Convection: The likely source of the medium-scale gravity waves observed in the OH airglow layer near Brasilia, Brazil, during the SpreadFEx campaign, *Ann. Geophys.*, *27*, 231–259.

Vadas, S. L., J. Yue, C.-Y. She, P. Stamus, and A. Z. Liu (2009b), A model study of the effects of winds on concentric rings of gravity waves from a convective plume near Fort Collins on 11 May 2004, *J. Geophys. Res.*, *114*, D06103, doi:10.1029/2008JD010753.

Waldock, J. A., and T. B. Jones (1987), Source regions of medium scale travelling ionospheric disturbances observed at mid-latitudes, *J. Atmos. Terr. Phys.*, *49*, 105–114, doi:10.1016/0021-9169(87)90044-4.

D. A. Krueger and C.-Y. She, Department of Physics, Colorado State University, Fort Collins, CO 80523, USA.

T. Li, School of Earth and Space Sciences, University of Science and Technology of China, 96 Jinzhai Road, Hefei, Anhui 230026, China.

H.-L. Liu, National Center for Atmospheric Research, P.O. Box 3000, Boulder, CO 80307-3000, USA.

W. Lyons, FMA Research, Yucca Ridge Field Station, 46050 Weld County Road 13, Fort Collins, CO 80524, USA.

T. Nakamura, Research Institute for Sustainable Humanosphere, Kyoto University, Uji, Kyoto, 611-0011, Japan.

S. C. Reising and J. Yue, Department of Electrical and Computer Engineering, Colorado State University, Fort Collins, CO 80523, USA. (jyue@lamar.colostate.edu)

P. Stamus and S. L. Vadas, CoRA Division, NorthWest Research Associates, 3380 Mitchell Lane, Boulder, CO 80301, USA.